Kovove Mater. 64 2026 119–132
DOI: 10.31577/km.2026.3.119

Effect of diamond coating on microstructure and mechanical properties of FeNiCrCuAl high-entropy alloy

Zhixin Wang[1], Jiangtao Li[1], Mengjie Pei[1], Mingxing Ma[2], Xiaozhe Cheng[1], Qian Zhang[1], Xiaoyan Guan[1], Huili Ding[1], Shaopei Jia[1], Qisong Li[1], Quan Huang[1]*

[1] *School of Materials Electronics and Energy Storage, Zhongyuan University of Technology, Zhengzhou, 451191, P. R. China*
[2] *School of Mechanical Engineering, Henan Polytechnic Institute, Nanyang 473000, P. R. China*

Received 27 February 2026, received in revised form 6 June 2025, accepted 11 June 2026

Abstract

Diamond-reinforced FeNiCrCuAl high-entropy alloys were fabricated by spark plasma sintering with 7 wt.% diamond. Titanium and chromium coatings were deposited on diamond surfaces via vacuum micro-evaporation, forming carbide coatings. FeNiCrCuAl HEA powders synthesized by gas atomization consist of a BCC solid solution phase and an AlNi phase. An FCC phase was observed in the SPS samples. Graphite phase was detected in the diamond-containing samples. The diamond surface coating significantly reduces the concentration of the graphite phase in the HEA matrix and contributes to the formation of metallurgical bonding between diamond and HEA matrix. Uncoated diamonds enhanced matrix hardness from 432.4 to 479.7 $HV_{0.5}$ through solid solution strengthening. Ti-coated diamonds exhibited optimal interfacial bonding, preserving bending strength at 410.0 MPa. Wear failure modes involved diamond spalling and matrix abrasion. Notably, Cr-coated diamond/HEA demonstrated superior wear resistance with an average friction coefficient of 0.15, attributed to thicker carbide-rich transition layers.

K e y w o r d s: high-entropy alloys, diamond, interface bonding, solid-solution strengthening

1. Introduction

High-entropy alloys (HEAs) are typically characterized by the inclusion of five or more alloying elements in equiatomic or near-equiatomic proportions. This multi-component composition leads to a relatively high mixing entropy [1]. To reduce the free energy of the system, the alloy favors forming stable solid solutions [2]. Consequently, the number of phases present in HEAs is significantly lower than the maximum number of equilibrium phases predicted by the Gibbs phase rule for alloy systems. The differences in atomic size, electron affinity, and chemical bond strength, which arise from the multi-component composition, lead to a large number of defects and heterogeneous interfaces within the microstructure of HEAs [3, 4]. All of these factors impede atomic diffusion. The sluggish diffusion effect in HEAs is beneficial for the development of grains that exhibit smaller sizes and more complex geometries [5], thereby endowing HEAs with exceptional high-temperature strength and stability. The lattice distortion induced by numerous defects, including vacancies, dislocations, and interstitial or substitutional atoms, disrupts the equilibrium state among atoms [6, 7]. These distortions contribute to lattice twists, elevate potential energy, inhibit the sliding deformation of dislocations, and ultimately enhance the mechanical strength and hardness of the HEA microstructure [8]. Common alloying elements incorporated into HEAs may include metallic elements with relatively low melting points, such as Fe, Co, Ni, and Cr, as well as those with high melting points, such as W, Mo, and V, and even non-metallic elements like C, B, and Si [9–15]. Through the intricate interactions among alloying elements and their atomic-scale coordination, various effects can be imparted on the microstructure of HEAs, thereby playing a significant role in enhancing the strength, wear resistance, cor-

*Corresponding author: e-mail address: quanhuang@zut.edu.cn

rosion resistance, and high-temperature performance [16–19].

Diamond has the characteristics of high hardness and wear resistance [20]. Often referred to as "industrial teeth", it is widely used in grinding tools, geological exploration, gem processing, and national defense industries. Common metal-based binders for diamonds include Cu-Sn-Ti, Ni-Cr, Fe-Ni--Cu-Sn, etc. [21–24]. Typically, diamond tools are fabricated through cold-pressing or hot-pressing sintering methods. However, the low sintering temperatures often result in the presence of numerous voids within the sintered samples. This condition can lead to the formation of defects, such as intermetallic compounds and interstitial phases, which are detrimental and adversely affect the structural stability of the diamond particles [25, 26]. Additionally, the constraints imposed by the alloy composition can result in significant fluctuations in expansion and contraction within the metal matrix when the cutting linear velocity of the diamond tool is excessively high [27]. This may lead to various failure modes, including chipping of cutting edges, thermal cracking, and plastic deformation of the diamond tool. The phase composition of HEAs primarily consists of solid solutions with simple structures [28]. The high-entropy effect inhibits the formation of brittle phases, such as intermetallic compounds in alloy microstructure, thereby enhancing the retention of diamond particles. Furthermore, HEAs exhibit superior hardness and wear resistance compared to conventional diamond binders, along with enhanced high-temperature strength and stability [29]. This can mitigate the occurrence of cracks or plastic deformation in diamond tools, which are typically induced by thermal expansion during high-speed cutting, thereby extending the service life of diamond tools. However, the substitution of conventional metal-based binders with high-entropy alloys (HEAs) presents several challenges. Notably, the elevated melting points associated with the preparation of HEAs and the potential alteration of diamond particle morphology due to the presence of elements such as iron (Fe), cobalt (Co), and nickel (Ni) within the HEAs may adversely affect the cutting ability of the diamond particles [30, 31]. In the present study, metal coatings were applied to the surface of diamond particles utilizing a vacuum micro-evaporation coating technique. The application of these coatings serves to prevent direct contact between the diamond particles and the HEAs, thereby facilitating the formation of a more robust metallurgical bond between diamond and HEA matrix. To elucidate the role of diamond surface coatings, this experiment produced diamond/HEA composites, Ti-coated diamond/HEA composites, and Cr-coated diamond/HEA composites through SPS, respectively, with the diamond mass fraction of 7 wt.%. The study analyzed the impact of diamond surface coatings and the methods of combining diamond particles with HEAs on the microstructure, mechanical properties, and wear resistance of the diamond/HEA composites, to identify the optimal processing conditions for FeNiCrCuAl HEA/diamond composites.

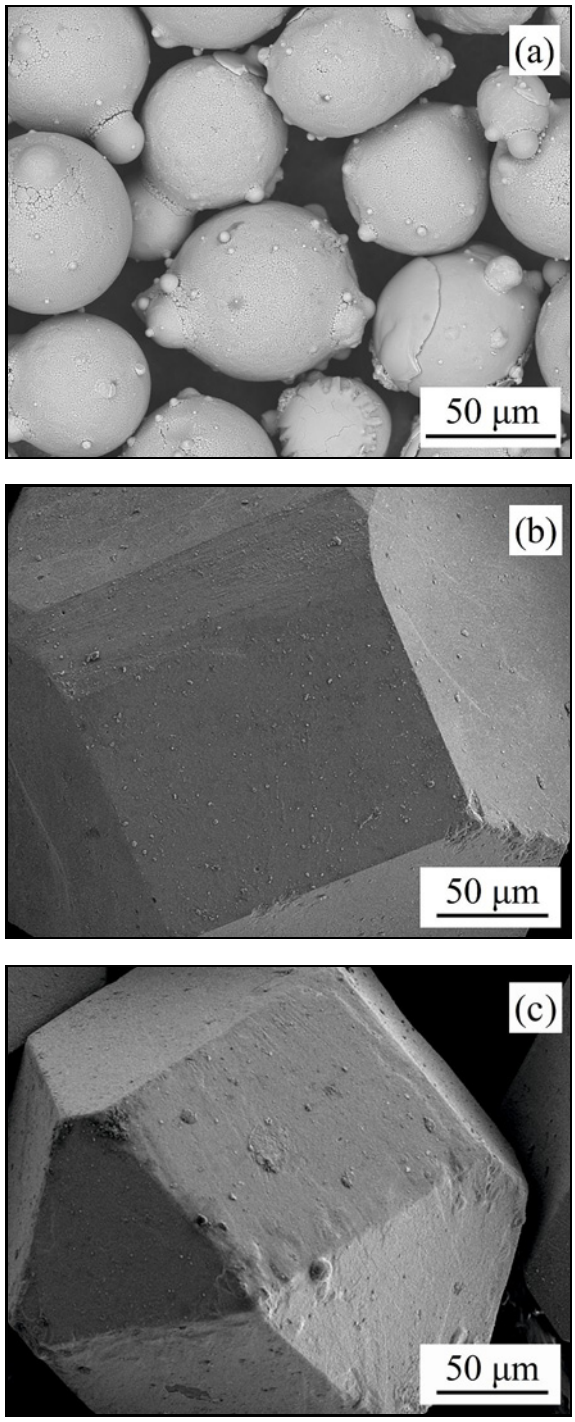

Fig. 1. SEM images of FeNiCrCuAl high-entropy alloy powders (a), Ti-coated diamond (b), and Cr-coated diamond (c).

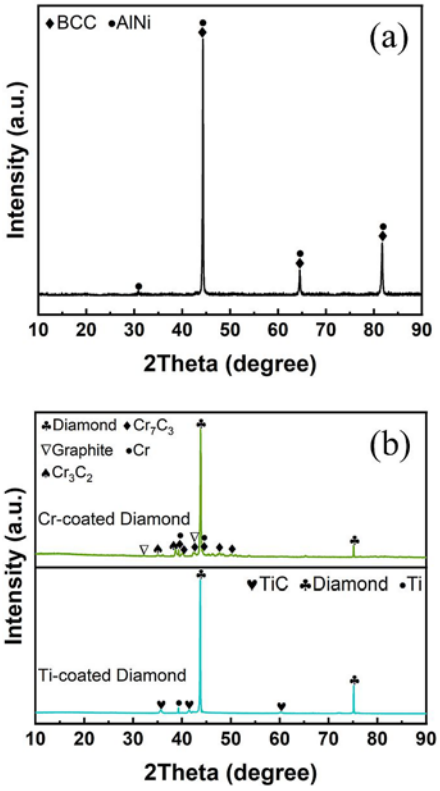

Fig. 2. XRD patterns of FeNiCrCuAl high-entropy alloy powders (a), and diamond coatings (b).

2. Materials and methods

2.1. Preparation and characterization of raw materials

The FeNiCrCuAl HEA powder, characterized by an equal atomic ratio, was synthesized through gas atomization using pure metal powders of iron (Fe), nickel (Ni), chromium (Cr), copper (Cu), and aluminum (Al), each exceeding 99.99 wt.% purity. The alloy powder had particle sizes ranging from 35 to 70 μm and an equal atomic ratio. As depicted in Fig. 1a, the average particle size of the resultant spherical HEA powder is approximately 60 μm. Fig. 2 presents the diffraction pattern of the FeNiCrCuAl HEA powder. The spherical powder produced via gas atomization demonstrates effective metallurgical bonding among the alloy constituents. The Body-Centered Cubic (BCC) structure solid solution phase and the AlNi phase were detected in the phase components of the pre-alloyed powder.

Ti and Cr coatings were applied to the surface of standard HWD5 synthetic diamond (average particle size is 70–80 mesh, provided by the Yellow River Cyclone), prepared using a vacuum micro-evaporation coating process, as illustrated in Fig. 3. The metal powders of Ti and Cr, both with a purity exceeding

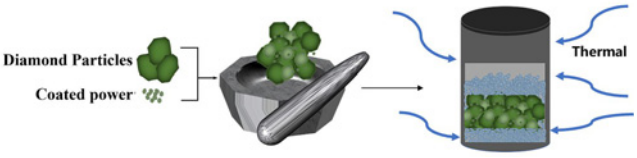

Fig. 3. Schematic diagram of the vacuum micro-evaporation coating process flow for diamond particles.

99.99%, were initially mixed with a hydrochloric acid-ethanol solution to activate the metal powders for the preparation of the coating powder. Subsequently, the diamond particles were thoroughly combined with the coating powder (the mass ratio is 5 : 1) in a corundum mortar. The resulting mixed powder was then loaded into a graphite crucible for the coating process. A 2–3 mm thick layer of coated powder was applied above and below the diamond mixture to establish a coating atmosphere under high-temperature conditions. The coating was conducted in a vacuum environment at a temperature of 850 ℃, with a holding time of 2 hours. The following chemical equation outlines the carbide reaction of Ti and Cr under atmospheric pressure, along with the initial reaction temperature:

$$\mathrm{C + Ti \rightarrow TiC} \quad \text{about } 900\,℃, \tag{1}$$
$$\mathrm{2\,C + 3\,Cr \rightarrow Cr_3C_2} \quad \text{about } 1100\,℃, \tag{2}$$
$$\mathrm{3\,C + 7\,Cr \rightarrow Cr_7C_3} \quad \text{about } 1130\,℃, \tag{3}$$
$$\mathrm{6\,C + 23\,Cr \rightarrow Cr_{23}C_6} \quad \text{about } 650\,℃. \tag{4}$$

According to the reaction temperature of Ti and Cr elements with C under the specified atmospheric pressure conditions, the experimental coating process was conducted at a temperature of 850 ℃. At this temperature, the theoretical reaction temperature for the formation of titanium carbide from Ti and C has not been achieved. Consequently, the majority of Ti that is absorbed onto the diamond surface is expected to exist in the form of pure metallic titanium rather than as a carbide. In contrast, Cr and C elements will react rapidly to form $Cr_{23}C_6$ at approximately 650 ℃. However, $Cr_{23}C_6$ cannot exist stably at elevated temperatures; thus, it gradually decomposes when the environmental temperature exceeds 850 ℃. As the temperature increases to around 1100 ℃, all $Cr_{23}C_6$ carbides decompose and transform into Cr_3C_2 and Cr_7C_3 carbides. At the coating temperature of 850 ℃ in this experiment, the theoretical formation temperatures for Cr_3C_2 and Cr_7C_3 carbides have not been reached. Therefore, the carbides resulting from the reaction between Cr and C are expected to predominantly exist as $Cr_{23}C_6$. As illustrated in Fig. 2, the XRD pattern of the coated diamond reveals the presence of Cr_3C_2 and Cr_7C_3 carbide phases in the reaction products of the Cr-coated diamond. Furthermore, the diffraction peak corresponding to $Cr_{23}C_6$ carbides was not detected

in the XRD pattern of the Cr-coated diamond, suggesting that $Cr_{23}C_6$ carbides have decomposed under these temperature and low-pressure conditions. Han et al. [32] successfully synthesized SiC refractory carbides at a temperature of 1200 ℃ using a low-pressure carbothermal shock reduction method. They noted that the low-pressure environment reduces the Gibbs free energy of the overall reaction, thereby allowing the initial temperature of the carbonization reaction to shift to a lower temperature range. In our experiment, the low-pressure conditions established through the vacuum micro-evaporation coating process effectively enabled the synthesis of TiC, Cr_3C_2, and Cr_7C_3 from the reaction of Ti and Cr with C at a temperature of 850 ℃, thereby decreasing the energy required for the carbonization reaction.

As illustrated in Figs. 1b,c, a continuous and uniform coating was successfully formed on the surface of the diamond through the vacuum micro-evaporation coating process. Notably, there was minimal exposure of the diamond substrate, indicating a lack of coating defects such as shedding or bare areas. Figure 2b presents the XRD patterns for Ti-coated diamond and Cr-coated diamond, both of them detected high-intensity diamond peaks at 43.9° and 75.3°. TiC carbide peaks were detected at 35.9° and 41.8° in the XRD pattern of the Ti-coated diamonds. Cr_7C_3 and Cr_3C_2 carbide peaks were detected in the XRD pattern for the Cr-coated diamonds. The presence of Ti and Cr metallic elemental peaks was also detected on the surfaces of the diamonds. The low-pressure environment during coating facilitates the formation of a favorable atmosphere around the diamond particles [33]. Furthermore, this environment reduces the Gibbs free energy associated with the reaction between titanium and chromium with carbon atoms, thereby promoting the formation of stable carbides. In short, these factors enhance the in-situ formation of carbide coatings on the diamond surfaces. The appearance of carbide peaks proves that a robust metallurgical bond has been established between the metal powder and diamond particles through bidirectional diffusion during the vacuum micro-evaporation coating process conducted at 850 ℃.

2.2. Preparation of FeNiCrCuAl HEA/diamond composites

FeNiCrCuAl HEA powders were combined with diamond, Ti-coated diamond, and Cr-coated diamond particles (each with a particle size of approximately 170 μm) at a mass fraction of 7 wt.% to fabricate HEA/diamond composite samples. The preparation flow chart is illustrated in Fig. 4. A planetary ball mill machine was employed to mill the mixture of diamond particles and HEA powder by wet ball milling. During the mixing process, anhydrous ethanol was

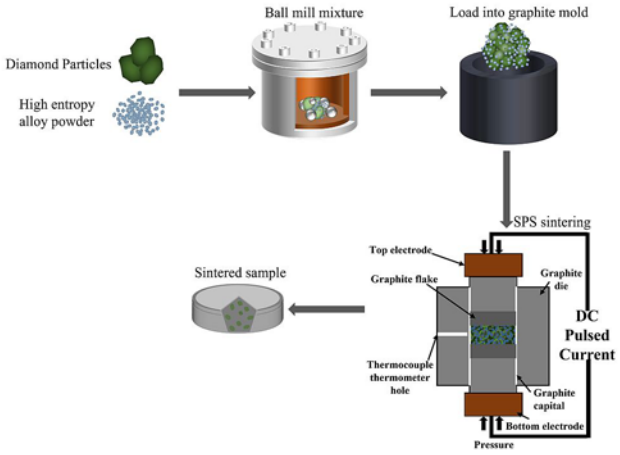

Fig. 4. Schematic diagram of the preparation process for FeNiCrCuAl HEA/diamond composites.

used as a grinding medium. An additional 5 wt.% of anhydrous ethanol, relative to the total mass of the FeNiCrCuAl HEA and diamond mixed powder, was added. The milling was conducted at a speed of 300 rpm for 2 hours. The mass ratio of corundum spheres to mixed powder was set at 10 : 1. Subsequently, the uniformly mixed powder was placed into a graphite mold with a diameter of 25 mm, and then dried in a constant temperature drying oven at 80 ℃ for 5 hours to eliminate any residual anhydrous ethanol from the mixed powder. This powder was then heated up to 1000 ℃ using a spark plasma sintering equipment (SPS-30, Chenxin Weike Industrial Technology Co. Ltd., Ningbo), following a specific heating rate (below 600 at 100 ℃ min^{-1}; from 600 to 900 ℃ at 50 ℃ min^{-1}; and from 900 to 1000 ℃ at 25 ℃ min^{-1}). After reaching the designated temperature, the samples were held for 10 minutes to complete the sintering process. A uniaxial pressure of 30 MPa was applied during sintering to enhance the density of the samples. The low voltage and high current heating method of SPS facilitated the attainment of relatively high temperatures within a short timeframe. Throughout the heating process, thermocouples and infrared temperature measurement devices were utilized to monitor the temperature within the graphite cavity, ensuring that excessive melting of the metal matrix did not occur due to excessively high temperatures, which could result in an uneven distribution of diamond particles within the FeNiCrCuAl HEA.

2.3. Microstructure and performance characterization

FeNiCrCuAl HEA/diamond composites were subjected to surface preparation using silicon carbide sandpapers of mesh sizes 400, 600, 800, and 1000 to eliminate the graphite layer formed during the sin-

tering process. The initial polishing of the sample surfaces aimed to achieve a complete and continuous surface. Subsequently, the samples underwent further polishing with a 2000-mesh diamond polishing plate. Flexural strength test samples were then cut from the 25 mm diameter samples using a DK7735 CNC wire-cutting machine (Aier CNC Machine Tools, Taizhou, China), ensuring that the strips exceeded a length of 12 mm. The cutting surfaces of these strips were polished to mitigate the risk of fractures due to stress concentration, which could arise from surface grooves or cracks. The crystal structure of the samples was analyzed using a Ultimal IV multifunctional X-ray diffractometer (Rigaku Corporation, Tokyo, Japan), employing Cu Kα diffraction lines. The scanning parameters included a speed of $10^\circ\,\mathrm{min}^{-1}$, a scanning range from 10° to 90°, a working voltage of 40 kV, and a working current of 20 mA. To investigate the microstructure and compositional distribution of the samples, a ZEISS Gemini SEM 360 field emission scanning electron microscope equipped with an Aztec X-Max 90 energy dispersive spectroscope (EDS) manufactured by Oxford Instruments (Oxford, UK). The hardness of the metal matrix within the composite materials was assessed using the HVS-1000 Vickers microhardness tester (Shangcai Testermachine Co., Ltd., Shanghai, China), with an applied load of 500 g and a testing duration of 15 seconds. To minimize errors attributable to human factors during the measurement process, hardness measurements were conducted within a 500 µm range around the diamond particles, and the average value was calculated from multiple measurements taken in each test area. The flexural properties of the samples were evaluated using an Instron 3369 universal testing machine (Instron Testing Equipment Trading Co., Ltd., Boston, USA) via the three-point bending method. The aspect ratio of the longitudinal section of the tested samples was maintained at 1.5 : 1, with a fulcrum span of 9 mm. The friction and wear characteristics of the samples were examined using the MFT-R4000 reciprocating friction and wear tester (Lanzhou Huahui Instrument Technology Co., Ltd., Lanzhou, China), applying a test load of 30 N, a sliding speed of $3\ \mathrm{m\,min}^{-1}$, and a test duration of 30 minutes. A Si_3N_4 ceramic ball (ø = 6 mm) served as the friction pair, and the wear morphology and area of the friction surface of the Si_3N_4 ceramic balls were observed later.

3. Results and discussion

3.1. Microstructure and phase analysis

Figure 5 illustrates the XRD patterns of FeNiCrCuAl HEA/diamond composites, which incorporate various coated diamonds alongside the FeNiCrCuAl HEA matrix. The data presented in the figure indicate that the microstructure of the FeNiCrCuAl HEA underwent a transformation from a BCC solid solution phase to a face-centered cubic (FCC) solid solution phase following sintering at 1000 ℃. Notably, both BCC and FCC dual-phase solid solution structures coexist within the microstructure of the FeNiCrCuAl HEA. Furthermore, the XRD diffraction patterns of each sample revealed the presence of metal phases enriched in aluminum (Al) and nickel (Ni) elements. Previous studies on HEAs containing Al and Ni suggest that this metal phase corresponds to an intermetallic compound with an $L1_0$ structure. When diamond particles were added to FeNiCrCuAl HEA, the dominant and subdominant diffraction peaks of the diamond were observed at diffraction angles of 43.9° and 75.3°, respectively. Additionally, the peak positions of the FCC and BCC phases exhibited a shift to lower angles across all samples. This shift may be attributed to the diffusion of carbon atoms from the diamond surface or metal atoms from the diamond surface coating into the solid solution of the FeNiCrCuAl HEA matrix. The XRD peak offsets in the FeNiCrCuAl HEA with Cr-coated diamonds displayed slight variations compared to those with uncoated diamonds and Ti-coated diamonds. It has been proved that Ti atoms deposited on the surface of diamonds also contribute to lattice distortion, in addition to the solid solution of carbon atoms within the microstructure of the HEAs. A graphite phase was detected in the FeNiCrCuAl HEA samples containing uncoated diamonds, which is attributed to the graphitization of diamonds during the sintering process. Both Cr in the FeNiCrCuAl HEA and Ti on the diamond surface are known to be carbide-forming elements, capable of reacting with carbon atoms to form carbides such as TiC and Cr_3C_2 [34, 35]. However, the XRD diffraction patterns of the FeNiCrCuAl HEA with added coated diamonds did not reveal any significant peaks corresponding to

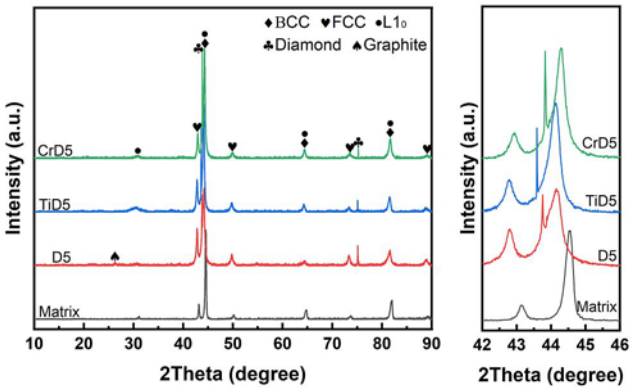

Fig. 5. XRD patterns of FeNiCrCuAl high-entropy alloy composites with differently pretreated diamonds.

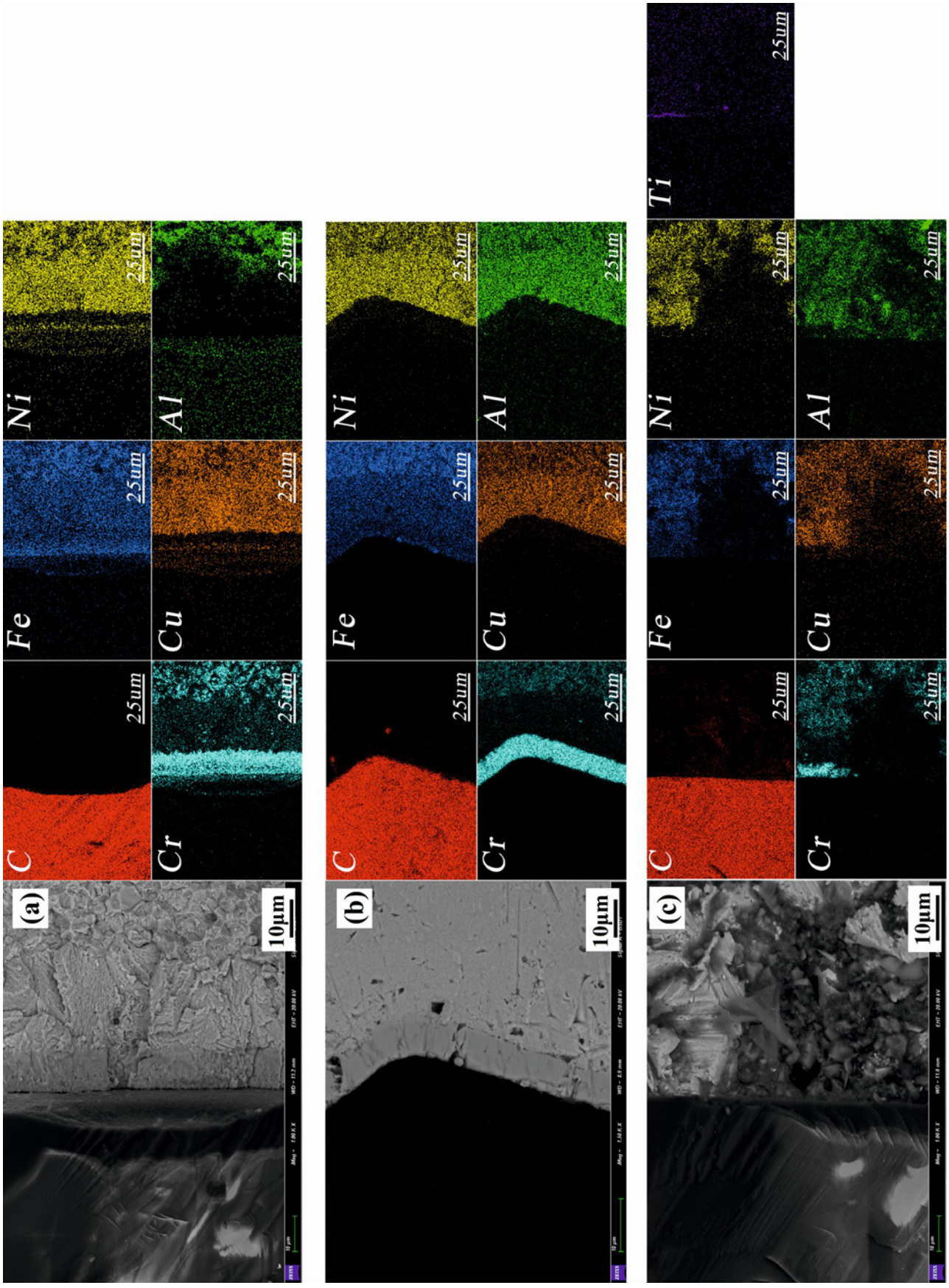

Fig. 6. SEM images and EDS patterns of FeNiCrCuAl high-entropy alloy composites with differently pretreated diamonds: (a) uncoated diamond, (b) Cr-coated diamond, (c) Ti-coated diamond.

graphite or carbide phases. This absence may be explained by the diamond surface coating, which isolates direct contact between diamond and the HEA matrix. This impedes diamond graphitization and carbon diffusion into the matrix. Consequently, only a minimal amount of carbon diffused into the HEA matrix, and the formed graphite or carbide phases are too insignificant to be detected. This observation indirectly suggests that the coating on the diamond surface effectively regulates the diffusion of carbon elements when diamonds are incorporated into the HEA matrix.

Figure 6 presents the scanning electron microscopy (SEM) and energy dispersive spectroscopy (EDS) patterns of the interface between diamond particles and HEAs in FeNiCrCuAl HEA/diamond composites, incorporating diamond, Cr-coated diamond, and Ti-coated diamond, respectively. The FeNiCrCuAl HEA/diamond composites prepared via SPS exhibit a robust metallurgical bond. The carbon atoms present on the surface of the diamond facilitate the enrichment of chromium (Cr) near the diamond particles. In the FeNiCrCuAl HEA matrix, uncoated diamond particles form a chromium transition layer with an average thickness of approximately 12 μm, whereas the transition layers formed by Ti-coated and Cr-coated diamond particles measure about 6 and 8 μm, respectively. The uncoated diamond particles contribute a greater number of carbon atoms to the HEA matrix during the sintering process, leading to a notable increase in the thickness of the chromium transition layer on the diamond surface. As illustrated in Fig. 6a, a significant interfacial gap is observed between FeNiCrCuAl HEA and diamond in the diamond/HEA composites, indicating that the bonding mechanism between diamond and HEA matrix is predominantly mechanical fitting. Conversely, in the presence of Ti-coated and Cr-coated diamond particles within the FeNiCrCuAl HEA, the barrier layer on the diamond surface eliminates the noticeable interfacial gap at the bonding interface, resulting in a tighter metallurgical bond between diamond and HEA matrix. Notably, the edges of the diamond particles remain integrity after sintering, with no evidence of erosion caused by high-temperature graphitization.

The results obtained from Energy Dispersive Spectroscopy (EDS) indicate that in diamond/FeNiCrCuAl HEA composites, there is a notable diffusion of carbon elements into the HEA matrix in proximity to the diamond particles. In the coated diamond/HEA composites, although diffusion of carbon elements into the HEA matrix also occurs, the concentration of carbon atoms that diffuse into the HEA is significantly reduced due to the presence of a barrier layer on the surface of the diamond. A uniform and continuous carbide coating is established on the diamond surface through the vacuum micro-evaporation coating process. This coating serves a dual purpose: it prevents direct contact between elements that facilitate diamond graphitization, such as iron, cobalt, nickel, and diamond particles, thereby diminishing the extent of diamond graphitization at elevated temperatures. Additionally, the diffusion barrier effect of titanium or chromium coatings adhered to the diamond surface effectively impedes the migration of free carbon atoms from the diamond surface into the HEA matrix [36]. The carbon atoms that partially penetrate the diamond surface coating attract the carbide-forming element chromium in the HEA matrix, leading to an enrichment of chromium near the diamond particles form a transition region around diamond particles. Both the diamond surface coating and the chromium transition region restrict the diffusion of carbon atoms from the diamond surface to the HEA matrix. It can be seen from the EDS element distribution pattern that in the bonding area between diamond and HEA, there are only the elements of the diamond surface coating and the Cr element, while there is almost no diffusion of other alloy elements in the HEA (such as Fe, Co, Ni, etc.) towards the diamond interface. The synergistic effect of the coating on the diamond surface and the chromium transition layer in obstructing the mutual diffusion of elements between diamond and HEA is the primary factor that ensures the preservation of the complete morphology of the diamond particles.

Figure 6c illustrates the Energy Dispersive Spectroscopy (EDS) element distribution diagram for the FeNiCrCuAl HEA with the addition of Ti-coated diamond particles. It is apparent that the titanium present on the surface of the Ti-coated diamond particles diffuses into the HEA matrix, exhibiting a gradient decrease in concentration. The atomic radius and thermal expansion coefficient of each element within the sample are provided in Table 1. The titanium atoms with a relatively large atomic radius, diffuse into the HEA matrix, resulting in the formation of a substitutional solid solution, which enhances the strength of the metallic framework composed of the HEA in proximity to the diamond particles. During the prolonged heat preservation stage of the vacuum micro-evaporation coating process, the coating gradually diffuses toward the diamond surface, where it interacts with the carbon atoms present on the diamond surface to form carbides. This interaction results in a more robust bond between diamond particles and HEA, thereby mitigating the crack defects that may occur at the interface due to discrepancies in thermal expansion coefficients. Furthermore, the carbide alloying elements within the FeNiCrCuAl HEA occupy the interface gaps created by the semi-coherent interface connection, which arises from the differing lattice structures between diamond and HEA by continuously growing on the surface of diamond coating [37, 38]. This process facilitates the formation of a tighter metallurgical bond between diamond particles

Table 1. The atomic radius and thermal expansion coefficient of each element

Element	C	Fe	Ni	Cr	Cu	Al	Ti
Thermal expansivity ($10^{-6}/°$)	0.8 ∼ 1.1	11.8	13.4	4.9	16.5	23.1	8.6
Atomic radius (pm)	77	126	124	130	128	143	147

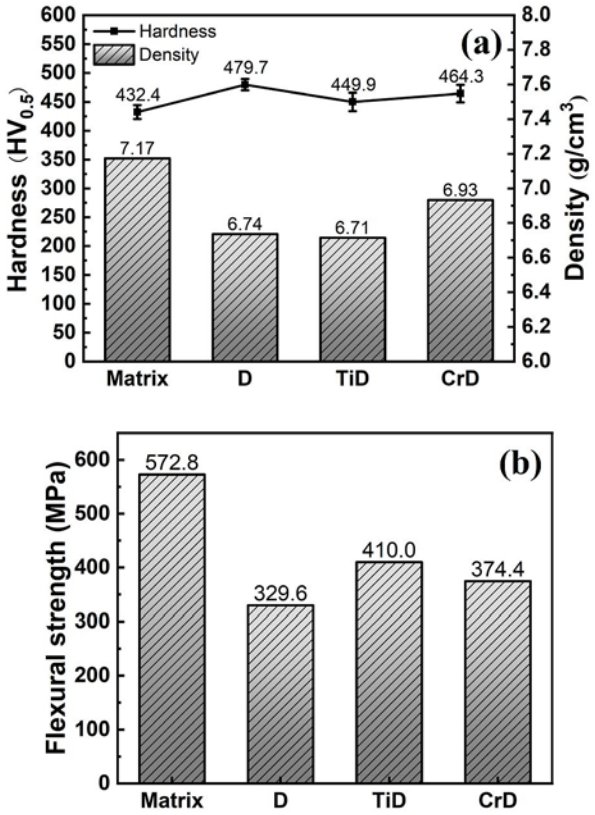

Fig. 7. Hardness and density of the high-entropy alloy matrix and composites (a) and flexural strength of the high-entropy alloy matrix and composites (b).

and HEA, thereby enhancing the retention capability of the FeNiCrCuAl HEA matrix for the diamond.

3.2. Mechanical properties

3.2.1 Hardness and bending strength

The density of the samples was measured using the Archimedes drainage method. Due to the density difference between diamond and HEA (the density of diamond is 3.52 g cm^{-3}, and the theoretical density of FeNiCrCuAl is 7.85 g cm^{-3}), the diamond with lower density was incorporated into the FeNiCrCuAl HEA matrix. Consequently, the resulting FeNiCrCuAl/diamond composites exhibit a lower density than FeNiCrCuAl HEA. Figure 7a shows the hardness and density of the HEA matrix, diamond, Ti-coated diamond, and Cr-coated diamond, respectively. The density of the FeNiCrCuAl HEA measured by the Archimedes drainage method is 7.25 g cm^{-3}. Upon the addition of 5 wt.% of diamond particles with different pretreatments to the HEA, the density of the composites decreases to different extents. Specifically, the densities of the FeNiCrCuAl HEA with the addition of Ti-coated diamond and Cr-coated diamond are 4.54 and 7.19 g cm^{-3}, respectively. The minimal density difference between titanium and diamond, along with the thinner coating thickness on the surface of the Ti-coated diamond leads to a few volume fractions of Ti attached to the surface of diamond particles. The density of composites containing Ti-coated diamond is approximate to that of composites with uncoated diamond. In contrast, chromium can combine with carbon atoms to form various carbides. As the temperature increases, these carbides ultimately develop into a thicker coating on the diamond surface. Furthermore, the significant density difference between chromium and diamond results in a marked increase in the density of Cr-coated diamond composites compared to those with Ti-coated diamond composites. For the diamond/FeNiCrCuAl HEA composites prepared in this work, the hardness properties are primarily influenced by the strengthening effects of the different diamond coatings incorporated into the FeNiCrCuAl HEA matrix, including solution strengthening, dispersion strengthening, lattice distortion, etc. The addition of diamond particles enhances the hardness properties of the FeNiCrCuAl HEA, however, there are slight differences in the effect of different coated diamond particles on the hardness properties of the HEAs. Notably, uncoated diamond particles yield the most significant improvement in the hardness properties of the FeNiCrCuAl HEA matrix. Analysis of the elemental distribution results, as depicted in Fig. 6, indicates a higher concentration of carbon atoms within the matrix of the diamond/HEA composite that lacks coating. This increase is primarily attributed to the diffusion of free carbon atoms generated by the graphitization of diamond particles during the sintering process. The carbon atoms with a small atomic radius, diffuse into the interstitial positions of the solid solution within the HEA matrix, resulting in lattice distortion in the microstructure of FeNiCrCuAl HEA. The dispersion of Cr_3C_2, Cr_7C_6, and other carbides formed through the interaction with the carbide-forming element chromium in FeNiCrCuAl HEA impedes the

migration and plastic deformation of dislocations, thereby significantly enhancing the hardness of the FeNiCrCuAl HEA matrix. In the case of diamond particles pre-coated with titanium and chromium, the coatings on the diamond surface impede the diffusion of carbon atoms generated by graphitization into the FeNiCrCuAl HEA matrix. Consequently, the concentration of carbon atoms within the FeNiCrCuAl HEA substrate is substantially diminished, thereby weakening the strengthening effects associated with solid solution strengthening and lattice distortion due to carbon atom diffusion. Nevertheless, in the coated diamond/FeNiCrCuAl HEA composites, the metal atoms and carbides present in the diamond surface coatings diffuse into the HEA substrate, forming substitutional solid solutions and carbide dispersion strengthening, which also contributes to the enhancement of the hardness performance of the FeNiCrCuAl HEA matrix. Combined with the XRD pattern of the Cr-coated diamond, as illustrated in Fig. 2b, reveals more obvious peaks corresponding to carbides in the Cr-coated diamond composite, indicating a greater availability of carbide particles to the FeNiCrCuAl HEA substrate and a more significant carbide dispersion-strengthening effect compared to the Ti-coated diamond composite.

Figure 7b illustrates the three-point flexural strength of the diamond/FeNiCrCuAl HEA composites. The flexural strength of the FeNiCrCuAl HEA reaches 572.8 MPa, however, the addition of diamond particles into the HEA leads to varying degrees of reduction in flexural strength. Specifically, the flexural strength of the Ti-coated diamond/FeNiCrCuAl HEA composite is measured at 410.0 MPa. In comparison, the flexural strength of the Cr-coated diamond/FeNiCrCuAl HEA composite decreases to 374.4 MPa. Furthermore, the flexural strength of the diamond/FeNiCrCuAl HEA composite further deteriorated and dropped to 329.6 MPa. The introduction of diamond particles increases the area of the heterogeneous interface within the FeNiCrCuAl HEA matrix. The bonding strength between diamond and FeNiCrCuAl HEA is inferior to the strength generated by the alloying of HEA powders. As a result, the diamond/HEA composite is more likely to fracture at the diamond-enriched interface, which contributes to a reduction in the composite's flexural strength. The coating applied to the diamond surface enhances the bonding strength between diamond and HEA matrix, thereby forming a more stable metallurgical bond between diamond and FeNiCrCuAl HEA. In the bonding transition region between the Cr-coated diamond and FeNiCrCuAl HEA, the excessively thick chromium transition region contains a higher concentration of carbide particles. Additionally, the mechanical strength of the Cr-rich region is lower than that of the FeNiCrCuAl HEA solid solution, which accounts for the observed lower flexural strength of the Cr-coated diamond/HEA composite compared to that of the Ti-coated diamond/HEA composite.

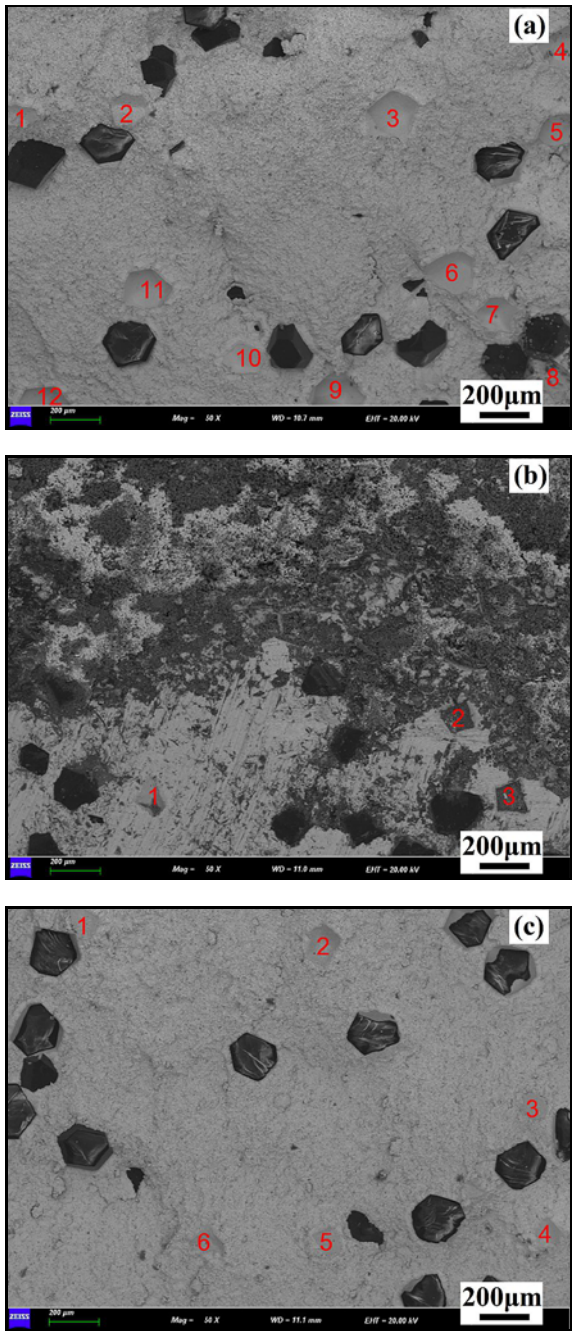

Fig. 8. SEM images of the fracture surfaces of high-entropy alloy composites with differently pretreated diamonds.

Figure 8 shows the SEM image of the fracture surface of the diamond/HEA composites with different pretreatments. Judging from the fracture morphologies of the diamond/FeNiCrCuAl HEA composites, the fracture surfaces of the FeNiCrCuAl HEA with diamond and Cr-coated diamond added are relatively

Table 2. The number of diamonds and vacancies on the fracture surfaces of high-entropy alloy composites with differently pretreated diamonds.

Type	Diamond	Ti-coated diamond	Cr-coated diamond
Diamond particle count	17	10	16
Vacancy number	12	3	6
Vacancy rate (%)	41.4	23.1	27.3

flat, while the fracture surface of the FeNiCrCuAl HEA with Ti-coated diamond added exhibits more serrated protrusions and has better toughness than the other two diamond/HEA composites. From the fracture morphology, the effect of diamond surface coating on enhancing the retention ability of the HEA matrix on diamond particles can be more intuitively demonstrated. Table 2 shows the vacancy rates of diamond particles on the fracture surfaces of three types of diamond/HEA composites. A significant number of pits, resulting from the detachment of diamond particles from the fracture surface, were observed on the fracture surface of the uncoated diamond/HEA composite. The vacancy rate, calculated as the ratio of the number of vacancies to the total number of diamonds on the fracture surface was 41.4 %. In contrast, the vacancy rates for the fracture surfaces of Ti-coated diamond and Cr-coated diamond/HEA composites were 23.1 and 27.3 %, respectively. The metal coating on the diamond surface creates a multi-layer structure of diamond-carbide-Cr transition layer- HEA at the bonding interface between FeNiCrCuAl HEA and diamond. This multilayer interface effectively fills the interface gap between diamond and HEA, mitigates the impact of non-metallurgical bonding associated with the semi-coherent interface present between diamond and HEA matrix, significantly enhances the bonding strength between diamond and FeNiCrCuAl HEA, and reduces the possibility of diamond particles detaching from the fracture surface. The titanium coating layer applied to the surface of diamond particles effectively reduces the thickness of the chromium enrichment region, which results from the diffusion of carbon atoms in proximity to the diamond particles. This reduction facilitates the incorporation of HEA solid solutions with enhanced strength around the diamond, thereby creating a robust metallic framework that improves the retention capacity of the diamond particles. However, when compared to the bonding strength achieved through the metallurgical bonding of alloying elements within the FeNiCrCuAl HEA matrix, the bonding strength between diamond and HEAs remains inadequate. This deficiency renders the interface between diamond and HEAs more susceptible to fracture under applied stress. Additionally, the presence of body-centered cubic (BCC) solid solution phases, intermetallic compounds, and other hard and brittle phases within the Cr-enrich region on the surface of the diamond particles contributes to the formation of a transition layer, which exacerbates stress accumulation in the vicinity of the diamond particles. Consequently, the diamond composite is predisposed to experience brittle fracture on the surfaces where the diamond particles are concentrated.

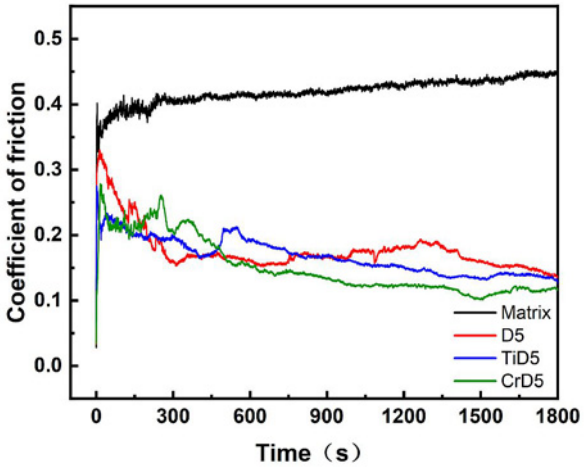

Fig. 9. Friction coefficients of diamond/FeNiCrCuAl high-entropy alloy composites with differently pretreated diamonds and FeNiCrCuAl high-entropy alloy.

3.2.2. Friction and wear properties

The primary forms of material wear failure are classified as abrasive wear and adhesive wear [39]. For diamond/FeNiCrCuAl HEA composites, the predominant causes of wear failure include the peeling of diamond particles and matrix wear. Figure 9 illustrates the results of friction and wear experiments conducted on FeNiCrCuAl HEA with varying pretreatments of diamond particles, as well as on FeNiCrCuAl HEA. Table 3 shows the average friction coefficients of the diamond/FeNiCrCuAl HEA composites at different stages of the friction and wear experiments. The friction coefficient curve indicates that FeNiCrCuAl HEA exhibits commendable wear resistance. After 300 seconds of testing, the friction coefficient stabilizes, yielding an average value of 0.42. In comparison, the addition of diamond particles into the FeNiCrCuAl HEA significantly reduces the friction coefficient of the composite. The presence of diamond particles enhances

Table 3. Average friction coefficient and wear area of Si_3N_4 ball in different periods in friction and wear tests

Sample	Wear area	Average coefficient of friction		
		0–1800 s	300–600 s	900–1800 s
Matrix	–	0.42	0.41	0.43
D	0.60	0.18	0.17	0.17
TiD	0.72	0.17	0.19	0.15
CrD	0.86	0.15	0.19	0.12

the wear resistance of the composite, which subsequently becomes the primary component subjected to wear after the relatively thin HEA substrate undergoes surface wear during the friction process. The friction coefficient of diamond/FeNiCrCuAl HEA composites experiences a rapid decline following the matrix wear phase. The superior cutting ability of the diamond particle edges contributes to the accelerated wear of the Si_3N_4 ball, resulting in considerable fluctuations in the friction curve. During the wear experiment phase from 300 to 600 seconds, the graphite generated from the pyrolysis of the diamond surface plays a significant lubricating role [40]. Uncoated diamond/HEA composites demonstrate the highest wear resistance, with an average friction coefficient of 0.17. After 900 seconds of wear testing, diamond surface coatings reveal notable advantages in enhancing the wear resistance of the composites. At this stage, the average friction coefficient of the Ti-coated diamond/HEA composite is recorded at 0.15, while the Cr-coated diamond/HEA composite exhibits an average friction coefficient of 0.12. The thicker coating on the surface of Cr-coated diamonds, which contains a higher concentration of carbide particles, contributes to the superior wear resistance of the Cr-coated diamond/HEA composite.

Figure 10 illustrates the wear morphology of FeNiCrCuAl HEA with the addition of diamonds subjected to various pre-treatments, following a 30-minute friction and wear test. Figures 10a–c show the surface wear morphology of the diamond/FeNiCrCuAl HEA composites. Figures 10d–f depict the wear contact surface morphologies of the corresponding Si_3N_4 balls. After undergoing a long-time friction and wear test, the diamond/FeNiCrCuAl HEA composites exhibit exposed diamond particles that interact with the Si_3N_4 ball to bear the subsequent wear. The frictional interaction between Si_3N_4 balls and diamond particles is identified as the primary cause of the scratches observed on the wear surfaces of the Si_3N_4 balls, as well as the detachment of diamond particles from the HEA matrix. Pits resulting from the detachment of diamond particles are evident on the wear surfaces of uncoated diamond/HEA composites. In contrast, the wear surfaces of the FeNiCrCuAl HEA composites containing Ti-coated or Cr-coated diamonds show minimal detachment of diamond particles. The diamond particles are securely embedded within the FeNiCrCuAl HEA matrix. The multi-layer transition structure formed by the metal coating on the surface of the diamond particles serves to bridge the gap created by the difference in thermal expansion between diamond and HEA, facilitating the formation of a more stable metallurgical bond. Compared to ordinary diamond particles, this configuration can endure greater stress impacts without resulting in the detachment of diamond particles. Table 3 shows the wear area of diamond/FeNiCrCuAl HEA composites on Si_3N_4 balls measured using ImageJ software.

The hardness of the FeNiCrCuAl HEA (432.4 $HV_{0.5}$) is significantly lower than that of the Si_3N_4 balls (1600 HV_{10}), indicating that the wear amounts of the diamond/HEA composites on Si_3N_4 balls are primarily influenced by the cutting ability of the diamond particles. The HEA composite with uncoated diamond exhibits a wear area of approximately 0.60 mm^2 on Si_3N_4 balls after a 30-minute friction and wear test. In contrast, the HEA composites with Ti-coated and Cr-coated diamonds demonstrate wear areas of 0.72 and 0.86 mm^2 on Si_3N_4 balls, respectively. The incorporation of a diamond surface coating enables the diamond particles to maintain their original shape during the sintering process. This prevents excessive blunting of the diamond particle edges due to graphitization at elevated temperatures, thereby significantly enhancing the cutting ability of the diamond/HEA composite on Si_3N_4 balls. When comparing the wear area of the Si_3N_4 balls with the average friction coefficient of the diamond/HEA composites, it is observed that samples exhibiting superior wear resistance correspond to larger wear areas on the Si_3N_4 balls. During the wear process involving Si_3N_4 balls and the diamond/FeNiCrCuAl HEA composites, the softer HEA matrix on the sample surface is worn away first, allowing the coating on the diamond surface to make initial contact with the Si_3N_4 balls. The thicker chromium transition layer on the surface of the Cr-coated diamond particles contains a higher concentration of carbide particles, which possess enhanced wear resistance. Additionally, the increased thickness of the chromium transition layer prolongs the contact process between diamond particles and Si_3N_4 balls,

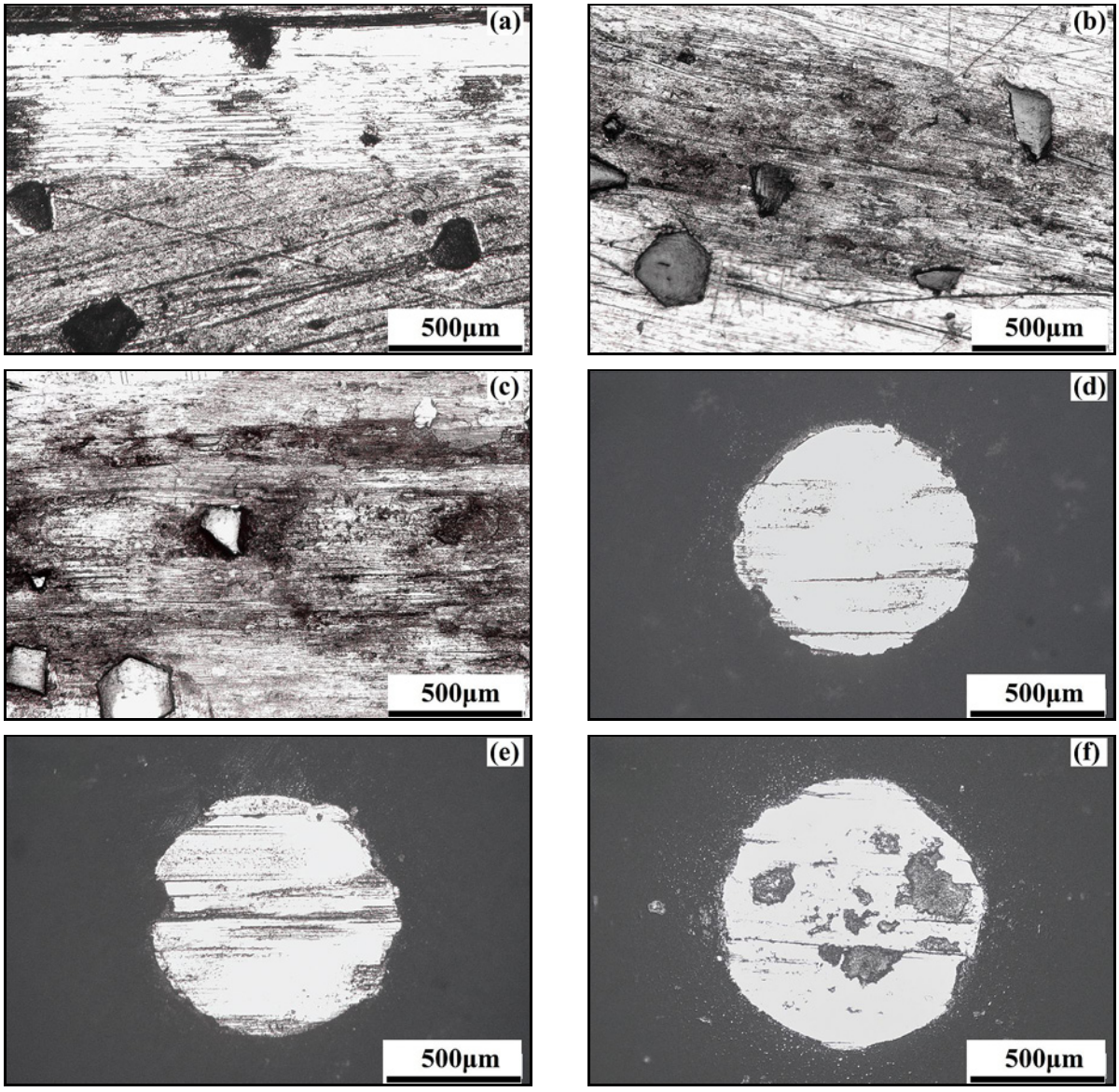

Fig. 10. Wear morphologies of differently pretreated diamond/high-entropy alloy composites and Si_3N_4 balls after friction and wear tests.

resulting in a greater amount of wear on the Si_3N_4 balls.

4. Conclusions

Titanium and chromium coatings were applied to the surface of diamond particles through a vacuum micro-evaporation coating process, resulting in the formation of in situ carbide coatings. The HEA matrix in diamond/FeNiCrCuAl HEA composites prepared via SPS established a robust metallurgical bond with the coated diamond particles. Additionally, Cr enrichment regions with thicknesses of approximately 6 and 8 μm were observed surrounding the Ti-coated and Cr-coated diamond particles, respectively.

The diamond surface coating reduces the density mismatch with the HEA, increasing the overall density of the composites. Furthermore, the coatings impede the diffusion of carbon atoms from the diamond surface into the HEA substrate, thereby reducing the solid solution and carbide dispersion strengthening effects that typically enhance matrix hardness. Although the in-situ formed carbides on the surface of Cr-coated diamonds during the coating process contribute to the hardness properties of the FeNiCrCuAl HEA, their strengthening effect is less pronounced compared to that of uncoated diamonds. Additionally, the coating promotes a more stable metallurgical bond between diamond and the HEA matrix. This compensates for the reduction in bending performance caused by gaps arising from thermal expansion mismatch.

The average friction coefficient of the FeNiCrCuAl HEA prepared by SPS is measured at 0.42. The addition of diamond significantly enhances the wear resistance of the FeNiCrCuAl HEA matrix. Graphite generated at elevated temperatures on the surface of uncoated diamonds serves a lubricating function during the initial stages of friction, resulting in a lower friction coefficient. Under the condition of prolonged wear, the coatings on the diamond surfaces tend to wear away prior to the degradation of the diamond particles themselves, thereby providing a protective effect that preserves the integrity of the diamond particles. Consequently, the FeNiCrCuAl HEA embedded with coated diamonds exhibits superior wear resistance. Notably, the presence of thicker coatings and an increased number of carbide particles surrounding the Cr-coated diamond particles contributes to the enhanced wear resistance of the FeNiCrCuAl HEA with Cr-coated diamonds. Furthermore, the wear areas of Si_3N_4 balls demonstrate a negative correlation with the average friction coefficient of the diamond/FeNiCrCuAl HEA composites. Among these composites, the Cr-coated diamond/HEA composite exhibiting the best wear resistance corresponds to the largest wear area observed on the Si_3N_4 ball.

Acknowledgements

This work was supported by the Henan Province Science and Technology Research Project (252102221051, 252102231020), Key Scientific Research Projects of Henan Province (25A510001), International Science and Technology Cooperation Project of Henan Province (242102520005).

References

[1] L. B. Zhang, T. T. Zuo, Z. Tang, M. C. Gao, K. A. Dahmen, P. K. Liaw, Z. P. Lu, Microstructures and properties of high-entropy alloys, Prog. Mater. Sci. 61 (2014) 1–93. https://doi.org/10.1016/j.pmatsci.2013.10.001

[2] Y. F. Ye, Q. Wang, J. Lu, C. T. Liu, Y. Yang, High-entropy alloy: challenges and prospects, Mater. Today 19 (2016) 349–362. https://doi.org/10.1016/j.mattod.2015.11.026

[3] D. Xu, Q. Zhang, X. Huo, Y. Wang, M. Yang, Advances in data-assisted high-throughput computations for material design, Mater. Genome Eng. Adv. 1 (2023) e11. https://doi.org/10.1002/mgea.11

[4] C. Hu, J. Zhang, Y. Zhang, C. Song, Q. Zhai, A great enhancement of both strength and plasticity in a dual-phase high-entropy alloy by multi-effects of high carbon addition, Mater. Des. 225 (2023) 111571. https://doi.org/10.1016/j.matdes.2022.111571

[5] J. Dąbrowa, M. Zajusz, W. Kucza, G. Cieślak, K. Berent, T. Czeppe, T. Kulik, M. Danielewski, Demystifying the sluggish diffusion effect in high entropy alloys, J. Alloys Compd. 783 (2019) 193–207. https://doi.org/10.1016/j.jallcom.2018.12.300

[6] S. Bai, N. Zhang, C. Gao, Y. Xiong, Defect engineering in photocatalytic materials, Nano Energy 53 (2018) 296–336. https://doi.org/10.1016/j.nanoen.2018.08.058

[7] M. X. Ma, Z. X. Wang, J. C. Zhou, C. Liang, D. M. Zhu, D. L. Zhang, Effect of Ti doping on microstructure and wear resistance of CoCrCuFeMn high-entropy alloys, J. Mech. Eng. 56 (2020) 134–142. https://doi.org/10.3901/JME.2020.10.110

[8] Q. Mao, Y. Liu, Y. Zhao, A review on mechanical properties and microstructure of ultrafine-grained metals and alloys processed by rotary swaging, J. Alloys Compd. 896 (2022) 163122. https://doi.org/10.1016/j.jallcom.2021.163122

[9] L. Zhang, T. Hashimoto, J. Yan, Machinability exploration for high-entropy alloy FeCrCoMnNi by ultrasonic vibration-assisted diamond turning, CIRP Ann. 70 (2021) 37–40. https://doi.org/10.1016/j.cirp.2021.04.090

[10] M. Abdullah, M. Mukarram, T. B. Yaqub, F. Fernandes, K. Yaqoob, Development of eutectic high entropy alloy by addition of W to CoCrFeNi HEA, Int. J. Refract. Met. Hard Mater. 115 (2023) 106300. https://doi.org/10.1016/j.ijrmhm.2023.106300

[11] N. Yurchenko, E. Panina, S. Zherebtsov, G. Salishchev, N. Stepanov, Oxidation behavior of refractory AlNbTiVZr0.25 high-entropy alloy, Materials 11 (2018) 2526. https://doi.org/10.3390/ma11122526

[12] H. Wang, W. Zhang, Y. Peng, M. Zhang, S. Liu, Y. Liu, Microstructures and wear resistance of FeCoCrNiMo high entropy alloy/diamond composite coatings by high-speed laser cladding, Coatings 10 (2020) 300. https://doi.org/10.3390/coatings10030300

[13] M. X. Ma, D. C. Zhu, Z. X. Wang, S. Z. Li, C. Dong, Effect of Zr addition on microstructure and wear properties of CoCrCuFeMn high-entropy alloy, Adv. Eng. Sci. 53 (2021) 1–8. https://doi.org/10.15961/j.jsuese.202100067

[14] L. Bai, R. Ding, Y. Lv, J. Chen, Effect of carbon on microstructure and mechanical properties of FeMnNiCrAl high entropy alloy, Mater. Charact. 202 (2023) 113020. https://doi.org/10.1016/j.matchar.2023.113020

[15] W. Kai, F. P. Cheng, C. Y. Liao, C. C. Li, R. T. Huang, J. J. Kai, The oxidation behavior of the quinary $FeCoNiCrSi_x$ high-entropy alloys, Mater. Chem. Phys. 210 (2018) 362–369. https://doi.org/10.1016/j.matchemphys.2017.06.017

[16] E. P. George, W. A. Curtin, C. C. Tasan, High entropy alloys: a focused review of mechanical properties and deformation mechanisms, Acta Mater. 188 (2020) 435–474. https://doi.org/10.1016/j.actamat.2020.01.027

[17] M. Ma, Z. Wang, C. Zhu, Y. Dong, L. Liu, L. Zhao, Q. Cui, D. Zhu, D. Zhang, Effect of Mn doping on microstructure and corrosion behavior of CoCuNiTi high-entropy alloy coatings, Crystals 15 (2025) 29. https://doi.org/10.3390/cryst15010029

[18] Y. Shi, B. Yang, P. K. Liaw, Corrosion-resistant high-entropy alloys: a review, Metals 7 (2017) 43. https://doi.org/10.3390/met7020043

[19] M. X. Ma, D. C. Zhu, Z. X. Wang, C. Liang, J. C. Zhou, D. L. Zhang, Microstructure and wear resistance of AlCoCrCuFe high-entropy alloy, Adv. Eng. Sci. 50 (2018) 208–216. https://doi.org/10.15961/j.jsuese.201701019

[20] W. Zhai, L. Bai, R. Zhou, X. Fan, G. Kang, Y. Liu, K. Zhou, Recent progress on wear-resistant materials: designs, properties, and applications, Adv. Sci. 8 (2021) 2003739. https://doi.org/10.1002/advs.202003739
[21] H. Liu, D. Duan, Q. Lin, C. Wang, Z. Jiang, Microstructure and performance of glass fiber metal composite-bonded diamond segment with Cu–Sn–Ti alloy, Ceram. Int. 48 (2022) 30670–30680. https://doi.org/10.1016/j.ceramint.2022.07.014
[22] S. Liu, M. Liu, T. Liu, Z. Zhang, E. Lu, Influence of brazing atmosphere on the characteristics, mechanical and thermal stress damage properties of diamond interface by molten Ni–Cr filler alloy, Vacuum 216 (2023) 112456. https://doi.org/10.1016/j.vacuum.2023.112456
[23] S. Ren, X. Shen, C. Guo, N. Liu, J. Zang, X. He, X. Qu, Effect of coating on the microstructure and thermal conductivities of diamond–Cu composites prepared by powder metallurgy, Compos. Sci. Technol. 71 (2011) 1550–1555. https://doi.org/10.1016/j.compscitech.2011.06.012
[24] Y. Hu, Y. Huang, F. Zhang, Y. Lin, P. Gao, Y. Zhou, X. Pan, Preparation and performance of high entropy alloy reinforced Cu-based bond diamond tool, Mater. Today Commun. 39 (2024) 108644. https://doi.org/10.1016/j.mtcomm.2024.108644
[25] W. Zhang, M. Zhang, Y. Peng, L. Wang, Y. Liu, S. Hu, Y. Hu, Interfacial structures and mechanical properties of a high entropy alloy–diamond composite, Int. J. Refract. Met. Hard Mater. 86 (2020) 105109. https://doi.org/10.1016/j.ijrmhm.2019.105109
[26] P. A. Loginov, A. D. Fedotov, S. K. Mukanov, O. S. Manakova, A. A. Zaitsev, A. S. Akhmetov, S. I. Rupasov, E. A. Levashov, Manufacturing of metal–diamond composites with high-strength $CoCrCu_xFeNi$ high-entropy alloy used as a binder, Materials 16 (2023) 1285. https://doi.org/10.3390/ma16031285
[27] M. Mukaida, J. Yan, Ductile machining of single-crystal silicon for microlens arrays by ultraprecision diamond turning using a slow tool servo, Int. J. Mach. Tools Manuf. 115 (2017) 2–14. https://doi.org/10.1016/j.ijmachtools.2016.11.004
[28] S. Guo, C. T. Liu, Phase stability in high entropy alloys: formation of solid-solution phase or amorphous phase, Prog. Nat. Sci.: Mater. Int. 21 (2011) 433–446. https://doi.org/10.1016/S1002-0071(12)60080-X
[29] J. Chen, X. Zhou, W. Wang, B. Liu, Y. Lv, W. Yang, D. Xu, Y. Liu, A review on fundamental of high entropy alloys with promising high-temperature properties, J. Alloys Compd. 760 (2018) 15–30. https://doi.org/10.1016/j.jallcom.2018.05.067
[30] J. X. Qin, X. G. Yang, C. F. Lv, Y. Z. Li, K. K. Liu, J. H. Zang, X. Yang, L. Dong, C. X. Shan, Nanodiamonds: synthesis, properties, and applications in nanomedicine, Mater. Des. 210 (2021) 110091. https://doi.org/10.1016/j.matdes.2021.110091
[31] M. Iravani, A. Khajepour, S. Corbin, S. Esmaeili, Preplaced laser cladding of metal matrix diamond composite on mild steel, Surf. Coat. Technol. 206 (2012) 2089–2097. https://doi.org/10.1016/j.surfcoat.2011.09.027
[32] Y. C. Han, M. L. Liu, L. Sun, S. Li, G. Li, W. S. Song, Y. J. Wang, Z. A. Nan, S. Y. Ding, H. G. Liao, Y. Yao, G. D. Stucky, F. R. Fan, Z. Q. Tian, A general method for rapid synthesis of refractory carbides by low-pressure carbothermal shock reduction, Proc. Natl. Acad. Sci. U.S.A. 119 (2022) e2121848119. https://doi.org/10.1073/pnas.2121848119
[33] H. Herman, S. Sampath, R. McCune, Thermal spray: current status and future trends, MRS Bull. 25 (2000) 17–25. https://doi.org/10.1557/mrs2000.119
[34] B. Sun, T. Fan, D. Zhang, T. Okabe, The synthesis and microstructure of morph-genetic TiC/C ceramics, Carbon 42 (2004) 177–182. https://doi.org/10.1016/j.carbon.2003.10.008
[35] K. Hirota, K. Mitani, M. Yoshinaka, O. Yamaguchi, Simultaneous synthesis and consolidation of chromium carbides (Cr3C2, Cr7C3 and Cr23C6) by pulsed electric-current pressure sintering, Mater. Sci. Eng. A 399 (2005) 154–160. https://doi.org/10.1016/j.msea.2005.02.062
[36] Y. Peng, Y. Kong, W. Zhang, M. Zhang, H. Wang, Effect of diffusion barrier and interfacial strengthening on the interface behavior between high entropy alloy and diamond, J. Alloys Compd. 852 (2021) 157023. https://doi.org/10.1016/j.jallcom.2020.157023
[37] M. I. De Barros, D. Rats, L. Vandenbulcke, G. Farges, Influence of internal diffusion barriers on carbon diffusion in pure titanium and Ti–6Al–4V during diamond deposition, Diamond Relat. Mater. 8 (1999) 1022–1032. https://doi.org/10.1016/S0925-9635(98)00439-7
[38] X. Y. Liu, W.G. Wang, D. Wang, D. R. Ni, L. Q. Chen, Z. Y. Ma, Effect of nanometer TiC coated diamond on the strength and thermal conductivity of diamond/Al composites, Mater. Chem. Phys. 182 (2016) 256–262. https://doi.org/10.1016/j.matchemphys.2016.07.030
[39] Y. Geng, J. Chen, H. Tan, J. Cheng, S. Zhu, J. Yang, Tribological performances of CoCrFeNiAl high entropy alloy matrix solid-lubricating composites over a wide temperature range, Tribol. Int. 157 (2021) 106912. https://doi.org/10.1016/j.triboint.2021.106912
[40] S. Shaji, V. Radhakrishnan, An investigation on surface grinding using graphite as lubricant, Int. J. Mach. Tools Manuf. 42 (2002) 733–740. https://doi.org/10.1016/S0890-6955(01)00158-4